Effect of Antenna Pattern on the Electromagnetic MIMO Communication

Yongxi Liu
School of Electronic and Information Engineering
Xi'an Jiaotong University
Xi'an, Shaanxi, 710049 China
liuyongxi@stu.xjtu.edu.cn

Ming Zhang
School of Electronic and Information Engineering
Xi'an Jiaotong University
Xi'an, Shaanxi, 710049 China
ming20.zhang@xjtu.edu.cn

Tengjiao Wang
Wireless Network RAN Research Department
Huawei Technologies CO., Ltd
Shanghai, 201206 China
wangtengjiao6@huawei.com

2022 IEEE 22nd International Conference on Communication Technology (ICCT) | 978-1-6654-7067-4/22/$31.00 ©2022 IEEE | DOI: 10.1109/ICCT56141.2022.10072734

***Abstract*—Using ideas from the Fourier plane-wave expansion of a channel model, we establish an electromagnetic (EM) channel model considering the effect of both antenna sides and propagation environment. The coupling effect between antennas becomes more and more serious with the reduction of antenna element spacing. Due to scan impedance mismatch caused by coupling effect, each individual element in an array suffers from the loss of reflection efficiency, which leads to the decrease in channel capacity. With numerical simulation, we show that under this revised model, channel capacity will not increase unboundedly as the number of antenna elements in a fixed-size array increases.**

***Index Terms*—MIMO Channel Modeling, embedded element pattern, size-limited antennas, Holographic MIMO**

I. Introduction

Over the past few decades, the development of information technology has led us to a more intelligent and convenient era [1]. In the meanwhile, the demand for information rate has rapidly increased [2]. In order to better balance the reliability and effectiveness of the information system while taking into account the actual needs, a tractable and accurate channel model is of great significance. As the research in the next generation of wireless communication goes deeper, massive multiple-input multiple-output (Massive MIMO) is considered to be the backbone of communication networks [3]–[6]. Its main idea is that using a large number of antenna elements can help improve channel capacity. However, this conclusion is based on the assumption that the antenna spacing between elements in an array is fixed, typically half of the wavelength [7]. Once the array size is fixed, whether a more compact structure can improve the channel capacity needs further discussion.

Motivated by the idea of densing antenna elements in a fixed-size array, Reconfigurable Intelligent Surface (RIS) provides a hardware solution to adjust the propagation characteristics of EM wave as well as use a large number of passive reflection elements in a limited space [8], [9]. With the development of RISs, EM properties of communication channel in the information system have attracted much attention. The combination between the traditional communication channel modeling and physical EM limit brings new insights into the capacity bound of a practical system [10], [11]. In [12], an approximated Fourier plane-wave series expansion of the EM channel is proposed to analyze the Degrees of Freedom (DoF) for a random channel under NLoS scenario. This model named Holographic MIMO (H-MIMO) is based on the EM wave propagation characteristics which establish the relationship between the current density in source array and electric field in receiving array. It is proved that DoF of an EM channel highly depends on array size. Moreover, under this channel model, the capacity can increase unboundedly as there are more antenna elements in the fixed-size array.

A channel model consists of three components: transmitting link, propagation environment and receiving link [13]. Inspired by H-MIMO in [12], this paper considers the effect of real antenna pattern instead of isotropic antennas. This substitution takes into account the coupling effect between array elements in an real array [14]. The effect of coupling can be decomposed into the consideration of embedded element patterns of individual antenna in the array [15], [16]. We show that once the realized gain of an array element is considered, the capacity cannot increase infinitely, instead, the return loss brought by scan impedance mismatch will lead to a declining behavior of channel capacity.

This work was supported in part by the Shaanxi Key Laboratory of Deep Space Exploration Intelligent Information Technology under Grant No. 2021SYS-04.

II. EM Channel Modeling for H-MIMO

In this section, the EM channel model considering the effect of antenna pattern is derived. This model is obtained from the Fourier plane-wave series expansion representing the angular coupling between source and receiver, but is more practical than the original model.

A. System Model

Consider two parallel placed square arrays in Fig. 1. Both are placed in xy plane. Antenna spacings in base station (BS) side are Δ_{sx}, Δ_{sy}, respectively, while those of user equipment (UE) side are Δ_{rx}, Δ_{ry}. Two square arrays have the same size ($L_{S_x} = L_{S_y} = L_{R_x} = L_{R_y} = L$), but different choice of antenna spacings (Δ_{sx}, Δ_{sy}), (Δ_{rx}, Δ_{ry})

978-1-6654-7067-4/22/$31.00 ©2022 IEEE

Authorized licensed use limited to: Tsinghua University. Downloaded on July 29,2026 at 09:16:19 UTC from IEEE Xplore. Restrictions apply.

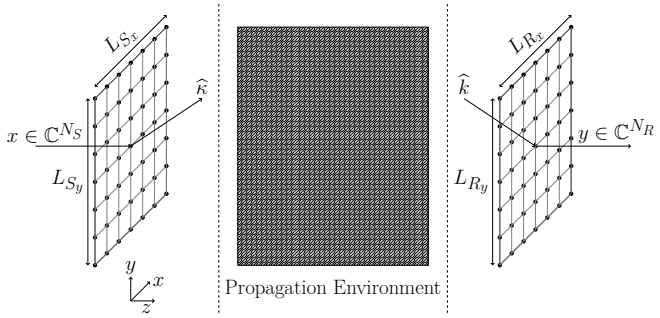


Fig. 1: Holographic communication system model.

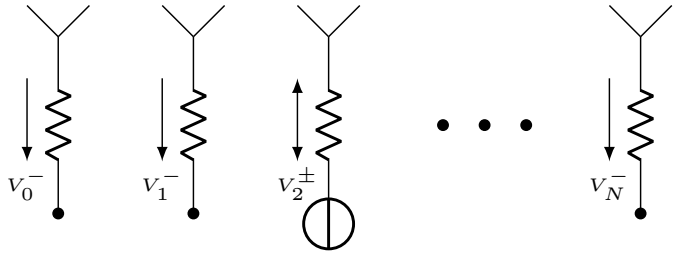


Fig. 2: Embedded element pattern for an N-element array.

will result in different antenna quantities N_s, N_r. In addition, $N_s = N_{sx}N_{sy}$, $N_r = N_{rx}N_{ry}$, where (N_{sx}, N_{rx}) are array antenna numbers in the x direction and (N_{sy}, N_{ry}) are array antenna numbers in the y direction.

BS and UE array antennas are indexed row-by-row with $n_s \in [1, N_s]$, $n_r \in [1, N_r]$. Local coordinate system is established at the center of the array. Therefore, the position of source antenna with index n_s in BS is

$$\mathbf{s}_{n_s} = [s_x, s_y, s_z]^{\mathrm{T}} = [i(n_s)\Delta_{sx}, j(n_s)\Delta_{sy}, 0]^{\mathrm{T}}, \quad (1)$$

where $i(n_s) = (-N_{sx} + \mathrm{mod}(n_s - 1, N_{sx}))/2$, $j(n_s) = (N_{sy} - \lfloor (n_s - 1)/N_{sy} \rfloor)/2$.

If a plane wave is incident on the source array with azimuth angle ϕ and polar angle θ, the source steering vector of this wave is

$$\begin{aligned} \mathbf{a}_s(\boldsymbol{\kappa}, \boldsymbol{s}) &= [a_{s,1}(\boldsymbol{\kappa}, \mathbf{s}), \cdots, a_{s,N_s}(\boldsymbol{\kappa}, \boldsymbol{s})]^{\mathrm{T}} \\ &= [e^{-\mathrm{j}\boldsymbol{\kappa}(\phi,\theta)\boldsymbol{s}_1}, \cdots, e^{-\mathrm{j}\boldsymbol{\kappa}(\phi,\theta)\boldsymbol{s}_{N_s}}]^{\mathrm{T}} \end{aligned} \quad (2)$$

where $\boldsymbol{\kappa}(\phi, \theta)$ is the wavenumber vector at BS side:

$$\boldsymbol{\kappa}(\phi, \theta) = \frac{2\pi}{\lambda}[\cos(\theta)\cos(\phi), \cos(\theta)\sin(\phi), \sin(\theta)]^{\mathrm{T}} \quad (3)$$

Similarly, we can define the receiver steering vector $\mathbf{a}_r(\boldsymbol{k}, \boldsymbol{r})$, $\boldsymbol{k}(\phi, \theta)$ is the wavenumber vector at UE side:

$$\begin{aligned} \mathbf{a}_r(\boldsymbol{k}, \boldsymbol{r}) &= [a_{r,1}(\boldsymbol{k}, \mathbf{r}), \cdots, a_{r,N_r}(\boldsymbol{\kappa}, \boldsymbol{r})]^{\mathrm{T}} \\ &= [e^{-\mathrm{j}\boldsymbol{k}(\phi,\theta)\boldsymbol{r}_1}, \cdots, e^{-\mathrm{j}\boldsymbol{k}(\phi,\theta)\boldsymbol{r}_{N_r}}]^{\mathrm{T}}, \end{aligned} \quad (4)$$

$$\boldsymbol{k}(\phi, \theta) = \frac{2\pi}{\lambda}[\cos(\theta)\cos(\phi), \cos(\theta)\sin(\phi), \sin(\theta)]^{\mathrm{T}}. \quad (5)$$

Two arrays communicate in the form of monochromatic scalar waves (i.e., with no polarization). The frequency of the wave is denoted by f_s and the corresponding wavelength is denoted by λ. We only consider NLoS scenario, which means the scattering environment between BS and UE is sufficient and there is no direct path.

B. Embedded Element Pattern

In transmitting mode, the antenna is driven by the voltage applied to its input terminals, while in receiving mode, by an incident electric field. However, when an antenna element is placed in an array, mutual coupling will change its radiation characteristic. Its radiation field is not only determined by the current on its surface, but also the current on other antennas. Therefore, it is necessary to redefine the antenna pattern in an array, which is called embedded element pattern (or scan element pattern, active element pattern).

Embedded element pattern is divided into different types according to the load state on the antenna port. In this paper, $f_{ld}(\theta, \phi)$ denotes the embedded element pattern taken with a feed at a single element in the array, while other elements terminated with matched loads [15], as shown in Fig. 2.

An array pattern $f_{array}(\theta, \phi)$ can be represented by embedded element pattern $f_{ld_i}(\theta, \phi)$ of each antenna element, that is

$$f_{array}(\theta, \phi) = \sum_i v_i f_{ld_i}(\theta, \phi), \quad (6)$$

where weighting coefficient v_i is the source voltage of each antenna element.

C. EM Channel Modeling

Based on the characteristics of EM wave propagation, [12] provides a 4D Fourier plane-wave representation of Holographic MIMO channel, which shows that the coupling coefficient between source array antenna j and receiver array antenna i is

$$\begin{aligned} [\mathbf{H}]_{ij} = \frac{1}{(2\pi)^2} \iiiint_{-\infty}^{\infty} & H_a(k_x, k_y, \kappa_x, \kappa_y) \\ & a_r(\boldsymbol{k}, \boldsymbol{r}_i) a_s(\boldsymbol{\kappa}, \boldsymbol{s}_j)\, dk_x dk_y d\kappa_x d\kappa_y, \end{aligned} \quad (7)$$

where

$$H_a(k_x, k_y, \kappa_x, \kappa_y) = \sqrt{S(k_x, k_y, \kappa_x, \kappa_y)} W(k_x, k_y, \kappa_x, \kappa_y) \quad (8)$$

is the angular response that maps every incident direction $\boldsymbol{\kappa}$ onto every receive direction $\mathbf{k}$, and $W(k_x, k_y, \kappa_x, \kappa_y) \sim \mathcal{N}_{\mathbb{C}}(0, 1)$ is a zero-mean, complex Gaussian random variable. $S(k_x, k_y, \kappa_x, \kappa_y)$ represents the bandlimited 4D power spectral density of the coupling efficient $[\mathbf{H}]_{ij}$, whose normalized value can be viewed as the power distribution in angular domain. It can be calculated by

$$S(k_x, k_y, \kappa_x, \kappa_y) = \left(\frac{\kappa\eta}{2}\right)^2 \frac{A^2(k_x, k_y, \kappa_x, \kappa_y)}{k_z(k_x, k_y)\kappa_z(\kappa_x, \kappa_y)}, \quad (9)$$

which shows that $S(k_x, k_y, \kappa_x, \kappa_y)$ is fully captured by the spectral factor $A(k_x, k_y, \kappa_x, \kappa_y)$. The spectral factor $A(k_x, k_y, \kappa_x, \kappa_y)$ denotes the impact of propagation environment. Isotropic scenario and non-isotropic scenario are two

Authorized licensed use limited to: Tsinghua University. Downloaded on July 29,2026 at 09:16:19 UTC from IEEE Xplore. Restrictions apply.

most commonly used environments. The former means EM wave propagates in all direction with identical response while the latter means EM wave is concentrated in several clusters. For simplicity, in this paper we only consider isotropic environment. In this case, $A(k_x, k_y, \kappa_x, \kappa_y)$ is a constant number.

However, (7) is established under the assumption that all antenna elements have isotropic pattern, that is, electric field gain of each antenna is the same in all directions and there is no coupling between array antennas. In practical application, isotropic antenna does not exit and array antennas have their own radiation characteristics. Therefore, we should consider the effect of embedded element pattern $f_{ld}(\theta, \phi)$ in channel modeling. In fact, entries of steering vectors $\mathbf{a}_s$ and $\mathbf{a}_r$ can be viewed as the embedded element pattern of an ideal isotropic antenna. To take into account the realistic array pattern, we can substitute $a_r(\boldsymbol{k}, \boldsymbol{r}_i)$ and $a_s(\boldsymbol{\kappa}, \boldsymbol{s}_j)$ in (7) with their own embedded element pattern $f_{ld}(\theta, \phi)$ directly:

$$[\mathbf{H}]_{ij} = \frac{1}{(2\pi)^2} \iiiint_{-\infty}^{\infty} H_a(k_x, k_y, \kappa_x, \kappa_y) f_{ld,i}(\boldsymbol{k}) f_{ld,j}(\boldsymbol{\kappa})\, dk_x dk_y d\kappa_x d\kappa_y, \tag{10}$$

where $\boldsymbol{\kappa}$ and $\boldsymbol{k}$ correspond to different angles (θ, ϕ).

If the array size (L_x, L_y) is large compared to wavelength λ (i.e., $L/\lambda \gg 1$), (10) can be approximately described by sampling (κ_x, κ_y) at $(2\pi m_x/L_{s,x}, 2\pi m_y/L_{s,y})$ and (k_x, k_y) at $(2\pi l_x/L_{r,x}, 2\pi l_y/L_{r,y})$, respectively:

$$[\mathbf{H}]_{ij} \approx \sum_{(l_x,l_y)\in\mathcal{E}_r} \sum_{(m_x,m_y)\in\mathcal{E}_s} H_a(l_x, l_y, m_x, m_y) f_{ld,i}(l_x, l_y) f_{ld,j}(m_x, m_y) \tag{11}$$

where (m_x, m_y), (l_x, l_y) correspond to the discrete grid index in wavenumber domain. Every index couple (m_x, m_y) or (l_x, l_y) can determine a unique angle (θ, ϕ). (11) is called 4D Fourier plane-wave series expansion of the channel.

After obtaining the approximation result of the entry $[\mathbf{H}]_{ij}$, the EM channel model can be further expressed as:

$$\mathbf{H} = \mathbf{F}_r \mathbf{H}_a \mathbf{F}_s^{\mathrm{T}}, \tag{12}$$

where

$$\mathbf{F}_r = [\boldsymbol{f}_{ld,1}, \cdots, \boldsymbol{f}_{ld,N_r}]^{\mathrm{T}}, \tag{13}$$

$$\mathbf{F}_s = [\boldsymbol{f}_{ld,1}, \cdots, \boldsymbol{f}_{ld,N_s}]^{\mathrm{T}}, \tag{14}$$

$\boldsymbol{f}_{ld}$ is an antenna pattern vector for different angles characteristic by index (m_x, m_y).

III. Numerical Simulation

In this section, we consider two identical arrays with the same size and use the revised EM channel model to calculate channel capacity. Each array is composed of several dipoles while three array structures are simulated. The dipole is made of Perfect Electric Conductor (PEC). Its radiation efficiency is 100%, the total efficiency η_0 of an antenna is composed of radiation efficiency η_{cd} and reflection efficiency η_r, i.e.:

$$\eta_0 = \eta_r \eta_{cd}, \tag{15}$$

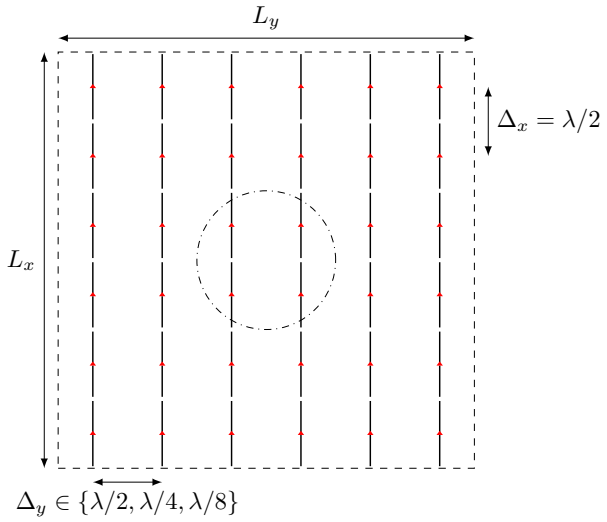


Fig. 3: Array structure diagram, dashed circle indicates the central elements whose simulation results are shown in TABLE I.

and thus only η_r affects η_0. η_r is determined by the impedance matching at the input terminal. In an array, the input impedance of an antenna is influenced by other antennas' current and the scanning angle of the array. This kind of influence is named scan impedance. As a result, it is hard to design an optimal matching network for an array. The total efficiency of antenna elements in a compact array cannot reach 100% [17].

As shown in Fig. 3, arrays are placed in xy plane and and are composed of half-wavelength dipoles. Array strucures are differed from the antenna spacing $\Delta_y \in \{\lambda/2, \lambda/4, \lambda/8\}$ while the spacing in x direction is fixed to $\Delta_x = \lambda/2$. The size of array is fixed to $L_x = L_y = 4\lambda$, different structures are labeled as 8×8, 8×16 and 8×32, respectively.

With different array structures, we can get embedded element patterns with electromagnetic simulation. Table I shows the simulation results of central antenna elements for each array. Embedded element pattern of central elements for different array structures have similiar shape, but their amplitude varies violently. Notice that although the center element in 8×32 array has the maximum directivity, its total efficiency is much lower than others, resulting a minimum realized gain. This implies that a more compact array suffers from a severer efficiency loss.

TABLE I: Maximum gain, directivity and total efficiency of central elements (shown in Fig. 3) for different array structures, results are derived from electromagnetic simulation.

Structure	$D_{\max}$[dBi]	$G_{\max}$[dBi]	Efficiency[%]
dipole (ref)	2.19	2.19	100
8×8	3.598	3.047	88.09
8×16	4.399	2.893	70.71
8×32	4.409	1.479	50.93

Authorized licensed use limited to: Tsinghua University. Downloaded on July 29,2026 at 09:16:19 UTC from IEEE Xplore. Restrictions apply.

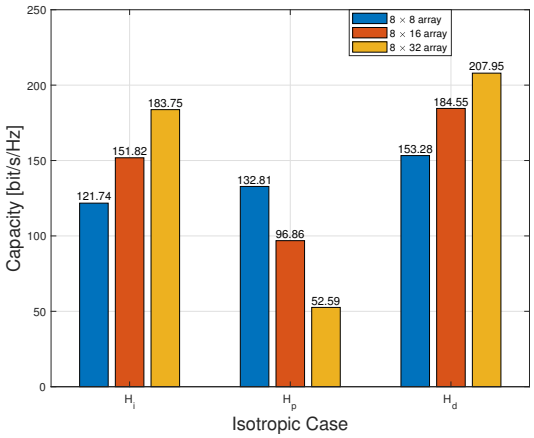


Fig. 4: Capacity of different array structures under different channel models.

Consider down-link communication, BS performs equal power allocation strategy to each antenna element and the total power $p_t = 10$W. Signal to noise ratio (snr) is set to 0 dB. Ergodic channel capacity can be evualuated by [18]

$$C = \mathbb{E}\left\{\log_2 \det\left(\mathbf{I}_{N_r} + \frac{\text{snr}}{N_s}\mathbf{H}\mathbf{H}^{\text{H}}\right)\right\}, \qquad (16)$$

where $\mathbf{H}$ is given by (12), $\mathbf{F}_r$ and $\mathbf{F}_s$ are derived from the simulation of embedded element patterns with different antenna spacings.

Three channel models are considered to calculate capacity, results of different array structures are shown in Fig. 4. $\mathbf{H}_i$ corresponds to an ideal array composed of isotropic antennas and there is no coupling between them. In this case, each antenna pattern is a sphere with unit gain, entries of $\mathbf{F}_r$ and $\mathbf{F}_s$ are determined by steering vector only. $\mathbf{H}_p$ corresponds to the array composed of dipoles where $\mathbf{F}_r$ and $\mathbf{F}_s$ are obtained from numerical computation. $\mathbf{H}_d$ is derived from embedded element directivity pattern. Key difference between $\mathbf{H}_p$ and $\mathbf{H}_d$ is that efficiency of antennas is 100% in the latter case.

From Fig. 4, we can see that channel capacity of an ideal array increases as antenna spacing decreases, this is because as antenna spacing gets closer, more antenna elements will be put into the fixed size array, providing more channels for an ideal comminucation system. However, this improvement is no longer effective if we consider a practical array geometry. The realized gain of embedded element pattern is severly affected due to the loss of efficiency brought by scan impedance mismatch, and the channel capacity decreases as antenna spacing decreases. If the scan impedance can be perfectly matched, the channel capacity can keep increasing. However, a 100% total efficiency cannot be reached for practical antennas [17], and thus the capacity result given by $\mathbf{H}_d$ is an ideal upper bound.

IV. Conclusion

In this paper, we derived an EM channel model which combines the antenna patterns and the propagation environment. We used the array simulation results to show that once the size of an antenna array is fixed, increase of the number of antennas cannot lead to an unbounded increase in channel capacity due to antenna element efficiency loss. To derive an optimal antenna spacing for a fixed-size array, future research should focus on the radiation efficiency limit and transmission efficiency limit of antennas in the array, which defines the upper bound of its realized gain. Improving transmission efficiency needs to solve the mismatch of scan impedance. Radiation efficiency is determined by the geometry and material of an antenna. Furthermore, the polarization of EM wave can also be considered to utilize the DoF of this revised EM channel model.

References

[1] Z. Chen, X. Ma, B. Zhang, Y. Zhang, Z. Niu, N. Kuang, W. Chen, L. Li, and S. Li, "A survey on terahertz communications," *China Communications*, vol. 16, no. 2, pp. 1–35, 2019.

[2] Z. Wan, Z. Gao, F. Gao, M. D. Renzo, and M.-S. Alouini, "Terahertz massive mimo with holographic reconfigurable intelligent surfaces," *IEEE Transactions on Communications*, vol. 69, no. 7, pp. 4732–4750, 2021.

[3] T. L. Marzetta, "Noncooperative cellular wireless with unlimited numbers of base station antennas," *IEEE Transactions on Wireless Communications*, vol. 9, no. 11, pp. 3590–3600, 2010.

[4] E. G. Larsson, O. Edfors, F. Tufvesson, and T. L. Marzetta, "Massive mimo for next generation wireless systems," *IEEE Communications Magazine*, vol. 52, no. 2, pp. 186–195, 2014.

[5] F. Rusek, D. Persson, B. K. Lau, E. G. Larsson, T. L. Marzetta, O. Edfors, and F. Tufvesson, "Scaling up mimo: Opportunities and challenges with very large arrays," *IEEE Signal Processing Magazine*, vol. 30, no. 1, pp. 40–60, 2013.

[6] F. Boccardi, R. W. Heath, A. Lozano, T. L. Marzetta, and P. Popovski, "Five disruptive technology directions for 5g," *IEEE Communications Magazine*, vol. 52, no. 2, pp. 74–80, 2014.

[7] E. Björnson, J. Hoydis, and L. Sanguinetti, "Massive mimo networks: Spectral, energy, and hardware efficiency," *Foundations and Trends® in Signal Processing*, vol. 11, no. 3–4, pp. 154–655, 2017.

[8] S. Hu, F. Rusek, and O. Edfors, "Beyond massive mimo: The potential of data transmission with large intelligent surfaces," *IEEE Transactions on Signal Processing*, vol. 66, no. 10, pp. 2746–2758, 2018.

[9] A. Sibille, "Mimo links mediated by reconfigurable intelligent surfaces," in *2021 15th European Conference on Antennas and Propagation (EuCAP)*, 2021, pp. 1–5.

[10] V. Shyianov, M. Akrout, F. Bellili, A. Mezghani, and R. W. Heath, "Achievable rate with antenna size constraint: Shannon meets chu and bode," *IEEE Transactions on Communications*, vol. 70, no. 3, pp. 2010–2024, 2022.

[11] M. Franceschetti, *Wave Theory of Information*. Cambridge University Press, 2018.

[12] A. Pizzo, L. Sanguinetti, and T. L. Marzetta, "Fourier plane-wave series expansion for holographic mimo communications," *IEEE Transactions on Wireless Communications*, pp. 1–1, 2022.

[13] D. Kelley and W. Stutzman, "Array antenna pattern modeling methods that include mutual coupling effects," *IEEE Transactions on Antennas and Propagation*, vol. 41, no. 12, pp. 1625–1632, 1993.

[14] W. L. Stutzman and G. A. Thiele, *Antenna Theory and Design*, 3rd ed. John Wiley & Sons, 2013.

[15] D. Pozar, "The active element pattern," *IEEE Transactions on Antennas and Propagation*, vol. 42, no. 8, pp. 1176–1178, 1994.

[16] D. Kelley, "Relationships between active element patterns and mutual impedance matrices in phased array antennas," in *IEEE Antennas and Propagation Society International Symposium (IEEE Cat. No.02CH37313)*, vol. 1, 2002, pp. 524–527 vol.1.

[17] W. Kahn, "Ideal efficiency of a radiating element in an infinite array," *IEEE Transactions on Antennas and Propagation*, vol. 15, no. 4, pp. 534–538, 1967.

[18] J. R. Hampton, *Introduction to MIMO communications*. Cambridge university press, 2013.

Authorized licensed use limited to: Tsinghua University. Downloaded on July 29,2026 at 09:16:19 UTC from IEEE Xplore. Restrictions apply.